NJC

Accepted Manuscript

This article can be cited before page numbers have been issued, to do this please use: Q. Kong, W. Zhuang, G. Li, Q. Jiang and Y. Wang, *New J. Chem.*, 2018, DOI: 10.1039/C8NJ01503A.

ROYAL SOCIETY OF CHEMISTRY

rsc.li/njc

View Article Online
DOI: 10.1039/C8NJ01503A

Journal Name

ARTICLE

Cation–anion interaction directed formation of functional vesicles and their biological application for nucleus-specific imaging

Received 00th January 20xx,
Accepted 00th January 20xx

DOI: 10.1039/x0xx00000x

www.rsc.org/

Qunshou Kong, Weihua Zhuang, Gaocan Li,* Qing Jiang* and Yunbing Wang

A strategy for construction of counterion-induced vesicles in aqueous media has been described by imidazolium salts with multiple imidazolium moieties and alkyl carboxylate counteranions. The spontaneous formation of vesicles can be achieved by the simple selection of the counteranion to satisfy the requirement of packing parameter for vesicle formation. Functional fluorescent vesicles can also be formed by introduction of an aggregation induced emission (AIE) fluorophore tetraphenylethene (TPE) as the core of the imidazolium salt **TPEI-C8**, which aslo exhibits highly specific nucleus imaging in living cells. Considering the distinct AIE characteristic of **TPEI-C8**, the aggregation induced strong fluorescence emission of **TPEI-C8** in the cell nucleus may be the main reason for the specific fluorescence images of the cell nucleus. This strategy for construction of functional vesicles reported in this study has shown great potential for construction of other functional vesicles.

Introduction

Vesicles are well-organized assemblies composed by amphiphilic substances containing a bilayer membranous structure with an aqueous void volume in the interior. In recent years, vesicles have been widely used in different fields from drug/gene delivery and artificial bioreactor to modes of biological membranes and so on.[1-5] However, these amphiphilic materials employed in the previous studies usually suffer from complex molecular structure and multi-step synthesis. As an important type of vesicle, catanionic vesicles have attracted more and more attention since the first report by Kaler et al.[6], due to their facile formation just by a simple mixing of cationic and anionic surfactants in aqueous solution. As a universal method, a great deal of work based on cationic–anionic surfactant mixtures has been done in the past years.[7-15] Nevertheless, some drawbacks remained such as the requirement of multiple surfactants and the need of fine regulation of the ratio of the cationic/anionic surfactant. Otherwise, the precipitation of the surfactants may occur due to the lack of electrostatic repulsion. Therefore, the development of a simple and efficient method to construct catanionic vesicles is in high demand for exploring other functional catanionic vesicles.

In recent years, fluorescent imaging has emerged as a powerful tool for monitoring the life activities of the organism with high spatial and temporal resolution[16-21]. However, the fluorescence quenching caused by the molecular aggregation in a high concentration may occur for conventional organic fluorescent molecules, which is known as the aggregation caused quenching (ACQ) effect.[22,23] In the year of 2001, Tang group firstly reported a new kind of fluorescent material and strong fluorescence can be observed in aggregated state owing to the restriction of intramolecular rotation, which is called aggregation-induced emission (AIE) effect.[22,24] Since then, a large number of AIE molecules have been developed and different types of AIE-based fluorophores such as tetraphenylethene (TPE) have been widely used for bioimaging with great cell imaging ability.[25-33]

In the past years, a great deal of work about vesicle formation induced by amphiphilic counterions has been studied by Kunz et al.[34-41] Recently, a strategy of counterion-induced vesicle (CIV) formation via simple imidazolium salts with EDTA as counterion has been reported by us and vesicles can be formed in the aqueous media.[42] In this work, a simple and efficient method for the formation of vesicles has been developed by taking advantage of multi-electric charged cations for vesicle formation. As we known, only micellar structures rather than vesicle assemblies can be formed for simple imidazolium halides or sodium alkyl carboxylate in the aqueous media.[43] Based on this vesicle construction method, vesicles with controllable size can be formed by selection of cations with multiple imidazolium moieties and simple counteranions of alkyl carboxylate anions. In this work, there is no need to regulate the ratio of cations and anions for the construction of vesicles and the vesicles can be formed spontaneously in the aqueous solution. Furthermore, functional fluorescent vesicles with AIE effect have also been constructed based on this method by adapting the widely used TPE structure as the emission moiety of the cation. More

National Engineering Research Center for Biomaterials, Sichuan University, 29 Wangjiang Road, Chengdu 610064, China E-mail: gaocanli@scu.edu.cn, jiangq@scu.edu.cn

†Electronic Supplementary Information (ESI) available: copies of NMR spectra of **TPAI-C6, TPAI-C8** and **TPEI-C8**, respectively. See DOI: 10.1039/x0xx00000x T

View Article Online
DOI: 10.1039/C8NJ01503A

importantly, these molecular assemblies triggered by the alkyl carboxylate counteranions can facilitate the TPE-based cations penetrating the cell membranes and exhibit highly specific targeting to the nucleus.

Results and discussion

Synthesis and characterization

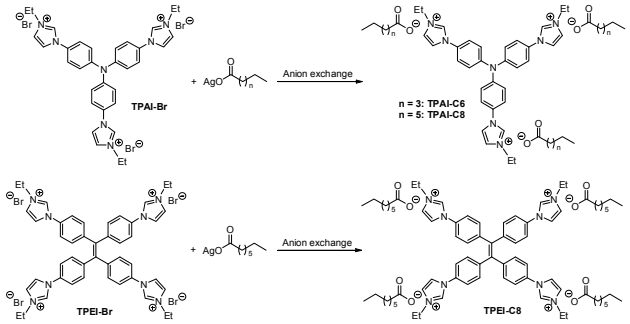

Scheme 1 Preparation of functional multiple imidazolium salts with alkyl carboxylate counterions.

These functional multiple imidazolium salts with different alkyl carboxylate counterions were obtained by a simple anion exchange process through the reaction of imidazolium bromide with silver alkyl carboxylate, followed by recrystallization from dichloromethane and diethyl ether to get the target compounds (Scheme 1). The chemical structures of these compounds were confirmed by NMR spectroscopy and high resolution mass spectrometry. All the target compounds exhibited good solubility in water and slight yellowish solutions could be formed at room temperature.

Self-assemble behaviors of TPAI with different counteranions

With these functional multiple imidazolium salts in hand, the self-assemble behaviors of **TPAI-C6** and **TPAI-C8** with relatively simple cationic structures were firstly determined to investigate the feasibility of our vesicle construction method and different measurements such as dynamic light scattering (DLS), transmission electron microscope (TEM) and the glucose leakage assay have been conducted in this study. The critical aggregation concentrations (CACs) of **TPAI-C6** and **TPAI-C8** were determined and CAC values about 10 mM and 7 mM were obtained for **TPAI-C6** and **TPAI-C8**, respectively (Fig. S1). To our delight, molecular assemblies of vesicles were formed spontaneously for both **TPAI-C6** and **TPAI-C8** in their aqueous solutions. As shown in Fig. 1a, DLS measurements indicated that nanoparticles with a hydrodynamic diameter of approximately 237 nm could be observed for **TPAI-C6**. When a counteranion with a longer alkyl chain was employed, nanoparticles with a larger size of approximately 478 nm could be formed for **TPAI-C8** (Fig. 1b).

Subsequently, vesicle morphological structures were directly observed through the TEM measurement. As illustrated in Fig. 1c, the TEM image acquired from the **TPAI-C6** showed the clear formation of the spherical aggregates with a diameter of about 180 nm. Similar to **TPAI-C6**, spherical aggregates with a diameter of about 390 nm were also observed for **TPAI-C8** (Fig. 1d). The size of these nanoparticles determined from TEM is relatively smaller than that from DLS, which was mainly attributed to the difference in the hydrodynamic diameter of the fully hydrated vesicles in solution and the dry samples in the collapsed state.

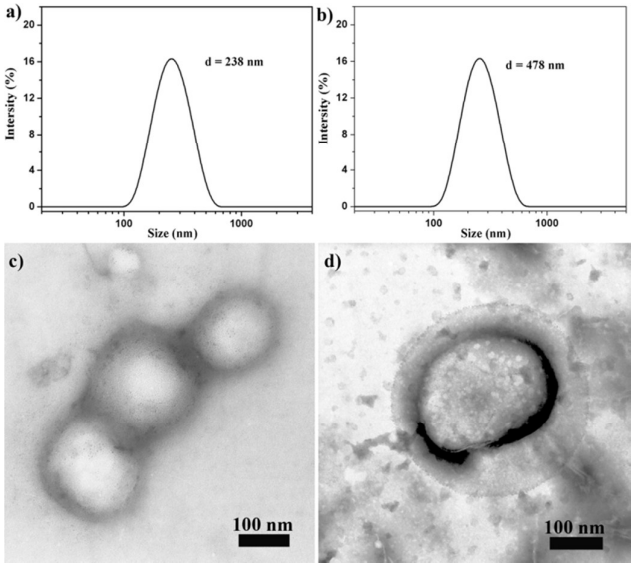

Fig. 1 Distribution of the hydrodynamic diameters of vesicles formed by (a) **TPAI-C6** (20 mM) and (b) **TPAI-C8** (10 mM) determined by DLS. (c) TEM micrographs of vesicles formed by **TPAI-C6** (40 mM) in aqueous solution on a carbon-coated copper grid without being stained with an aqueous solution of 2% phosphotungstic acid. (d) **TPAI-C8** (10 mM) in aqueous solution on a carbon-coated copper grid stained with an aqueous solution of 2% phosphotungstic acid.

As we know, an important characteristic of vesicles different from micelles is that vesicles have a hydrophilic cavity, in which water-soluble compounds can be trapped. To gain further confirmation of the vesicle formation in the aqueous solution, the glucose leakage assay, entrapment experiment of water-soluble glucose, was then conducted.[44] The glucose can be trapped into the vesicles in the process of the vesicle formation, while the glucose leakage takes place from the disrupted vesicles by the addition of detergent such as Triton X-100. Subsequently, a series of fast enzyme-catalyzed reactions including phosphorylation and oxidization are involved for the escaped glucose and the nicotinamide adenine dinudeotide phosphate (NADP) is also reduced quantitatively to the corresponding NADPH, which exhibits a typical absorbance at 340 nm and correlates directly with the amount of glucose efflux. Given this process is very fast, the release of entrapped glucose can be monitored by determine the increase of the absorbance intensity at 340 nm.

The vesicles of **TPAI-C8** were selected as a mode to carry out the entrapping experiment. The glucose-loaded vesicle solution with a total concentration of 300.0 mM for glucose was prepared by adding glucose directly into the tested solution of **TPAI-C8** at room temperature. After this mixture

DOI: 10.1039/C8NJ01503A

was vortexed for 3h at room temperature, the free glucose was removed through a gel column of sephadex G-50, hexokinase, glucose-6-phosphhate dehydrogenase, NADP, ADP, and ATP were added into the vesicle solution. As shown in Fig. 2a, a weak absorbance at 340 nm could be observed before the addition of Triton X-100. As a contrast, the vesicle structure could be destroyed by the addition of Triton X-100 and the rapid release of encapsulated glucose resulted into a sharp increase of the absorbance in the 340 nm (Fig. 2a). This observation of the efficient entrapment of the great amount of glucose demonstrated clearly the spontaneous formation of vesicles for **TPAI-C8** in its aqueous solution. Furthermore, a long-term stability of the entrapment of glucose could be observed and the total release of glucose was less than 45% even after 7 day (Fig. 2b), which made this vesicle system would be a promising candidate for high-efficiency and long-term encapsulation of hydrophilic contents.

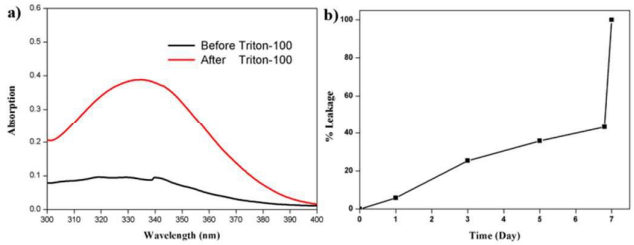

Fig. 2 (a) Comparison of the absorbance spectra of glucose-loaded vesicles before and after adding Triton X-100 (5% v/v). (b) Percent leakage of glucose from CIVs over time. The vesicles were lysed at the 7th day upon addition of Triton X-100.

Construction of functional fluorescent vesicles with AIE effect

Our current method for construction of vesicles is simple, yet capable of developing other functional fluorescence vesicles. Tetraphenylethene (TPE), as a classic AIE molecule, exhibits intense fluorescent emission in the aggregate state. As shown in Scheme 1, the functional imidazolium salt **TPEI-C8** with octanoate anion as counteranion and TPE as the molecular core has been developed with a fluorescence quantum yield of 0.25 and the fluorescence lifetime of 9.76 ns in its aggregate state. The critical aggregation concentration (CAC) of **TPEI-C8** was also determined and CAC value about 0.45 mM was obtained **TPEI-C8** (Fig. S1). As expected, functional fluorescent vesicles could be formed spontaneously for **TPEI-C8** in its aqueous solution, which was determined by DLS and TEM measurements. As shown in Fig. 3, a hydrodynamic diameter of approximately 369 nm and a mean diameter of around 220 nm could be obtained from the analysis of DLS and TEM, respectively. Similar to **TPAI-C6** and **TPAI-C8**, the relatively smaller vesicle size determined from TEM for **TPEI-C8** was mainly due to the difference states of these vesicles of the fully hydrated state and the collapsed state. The AIE active fluorescence emission of this functional imidazolium salt **TPEI-C8** was investigated subsequently. Once the molecular self-assemble of **TPEI-C8** occurred by adding the poor solution, the TPE groups were restricted and strong fluorescent emission could be observed due to the AIE effect (Fig. S2).

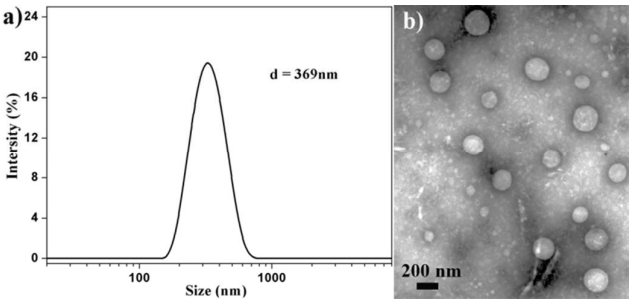

Fig. 3 (a) Distribution of the hydrodynamic diameters of CIVs formed by **TPEI-C8** in aqueous solution (2.0 mM); (b) TEM micrograph of CIVs formed by **TPEI-C8** in aqueous solution (2.0 mM) on a carbon-coated copper grid stained with an aqueous solution of 2% phosphotungstic acid.

Nucleus-specific fluorescent imaging

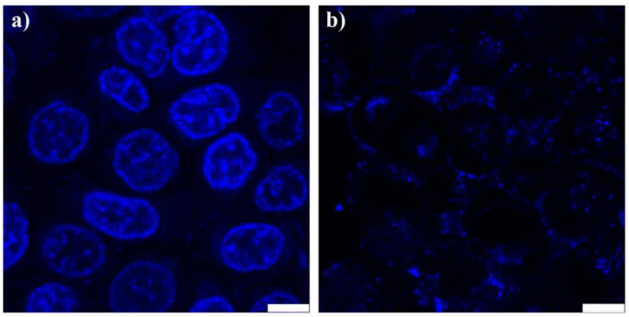

Fig. 4 Confocal images of Hela cells cultured with **TPEI-C8** and **TPEI-Br** at the concentrations of 50 μM: (a) **TPEI-C8** under irradiation at 405 nm (λ_{em} = 420-470 nm), (b) **TPEI-Br** under irradiation at 405nm (λ_{em} = 420-470 nm). Scale bar: 10 μm.

With this fluorescent AIE imidazolium salt of **TPEI-C8** in hand, biological application of this functional imidazolium salt for bioimaging was investigated. The Hela cells were cultured and incubated with 50 μM **TPEI-C8** and 50 μM **TPEI-Br** for 4h. Then, the cells were washed with fresh PBS for 3 times. Afterwards, the process of the cell imaging was observed by the confocal laser microscopy. To our delight, this functional imidazolium salt **TPEI-C8** could penetrate the cell membranes and label Hela cells in the location of the nucleus with a bright blue emission (Fig. 4a). However, only a very weak blue emission could be observed for imidazolium salt **TPEI-Br** with bromide as counteranion during the cell imaging process (Fig. 4b), which suggested that the octanoate anion and corresponding molecular self-assemble structures might play key roles in the penetration of the cell membranes for these imidazolium salts. Subsequently, the specific localization in nucleus was confirmed by the co-staining experiments of Hela cells with **TPEI-C8** and red-fluorescent tracker **Reddot1** (Fig. 5 and Fig. S3). As shown in Fig. 5c, the blue fluorescence images of **TPEI-C8** and the red fluorescence images of **Reddot1** collected from different channels overlapped very well. After calculation using Image-Pro Plus software, Pearson's coefficient (R_r = 0.83) and

View Article Online
DOI: 10.1039/C8NJ01503A

Manders's coefficients (m_1 = 1.00 and m_2 = 1.00), the parameters quantifying the staining region overlap for the blue and red fluorescence images, were obtained respectively, which clearly demonstrated the specific targeting to the nucleus of living cells similar to the reported literatures.[45,46] Although the mechanism is not clear, we assumed that electrophoretic force and suitable lipophilicity triggered by the multiple imidazolium moieties and octanoate anion might be the major driving force for **TPEI-C8** to penetrate the cell membrane and precisely target to the nuclelus.

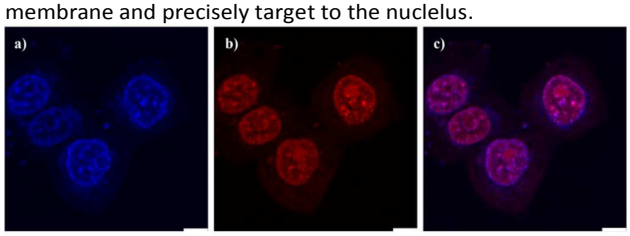

Fig. 5 Co-staining of Hela cells with **TPEI-C8** and **Reddot1**: (a) **TPEI-C8** (50 μM) for 4 h (λ_{ex} = 405 nm, λ_{em} = 420−470 nm); (b) **Reddot1** for 5 min (λ_{ex} = 633 nm, λ_{em} = 650−670 nm); (c) panels (a) and (b) merged; and (d) bright-field image. Scale bar: 5 μm.

Cytotoxicity is another important factor for the cell imaging, and the cytotoxicity of **TPEI-C8** was evaluated using MTT assays. As shown in the Fig. 6, no obvious toxicity could be observed for the cultured Hela cells with **TPEI-C8** at different concentration, and up to 85% of the cultured Hela cells could survive at a concentration even up to 80 μM after incubation for 24 h, showing better biocompatiability comparing the reported TPE based Luminogen.[26]

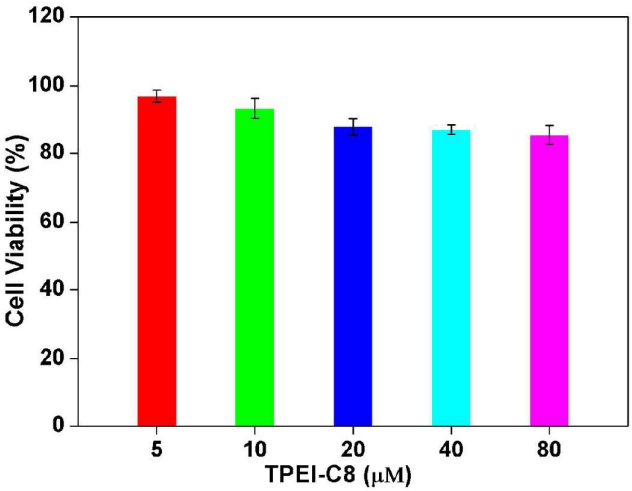

Fig. 6 Growth of Hela cells in the presence of different concentrations of **TPEI-C8** after 24 h incubation.

Conclusions

In summary, a strategy for construction of counterion-induced vesicles in aqueous media by imidazolium salts with multiple imidazolium moieties and alkyl carboxylate counteranions has been developed. The formation of vesicles is mainly triggered by the counteranion to satisfy the requirement of packing parameter for vesicle formation. This counterion-induced vesicle formation strategy is also capable of developing functional fluorescent vesicles by introduction of an AIEgen tetraphenylethene (TPE) as the core of the imidazolium salt **TPEI-C8**. This functional imidazolium salt **TPEI-C8** exhibits highly specific nucleus imaging in living cells and the aggregation induced strong fluorescence emission of **TPEI-C8** in the cell nucleus may be the main reason for the specific fluorescence images of cell nucleus. The cation–anion interaction directed functional vesicle formation strategy reported herein would provide new guidelines for the development of other novel functional vesicles.

Experimental section

General remarks

NMR spectra were obtained on a Bruker AV II-400. The ^{1}H NMR spectroscopy chemical shifts were measured relative to D_2O-d_2 as the internal reference (D_2O-d_2: δ = 4.79 ppm). The ^{13}C NMR spectroscopy chemical shifts were given using $CDCl_3$-d and CDOD-d_4 as the internal standard ($CDCl_3$: δ = 77.16 ppm and CDOD-d_4: δ = 49.86 ppm). Glucose leakage assay was monitored on a Cary 50 Bio UV−vis spectrometer. TEM studies were carried out using a HITACHI H-600 instrument, operating at 75 kV. DLS experiments were recorded using a Malvern Zeta sizer Nano ZS particle analyser instrument. Cell experiment was observed under confocal laser scanning microscopy (CLSM, ZEISS, LSM 780) and flow cytometry (BectoDickinson, USA).

Materials and reagents

Chemicals: Unless otherwise noted, all reagents were obtained from commercial suppliers and used without further purification. **TPAI-Br** and **TPEI-Br** were synthesized according to published procedures.[47,48]

Typical Preparation of Counterion-Induced Vesicles: TPAI-C8 (845.0 mg, 0.1 mmol) was added into 10.0 mL of deionized water at room temperature. The resulting solution was then left to stand and the vesicles formed spontaneously within minutes.

Glucose-leakage assay: Glucose-entrapping vesicles were prepared by adding **TPAI-C8** into the 300.0 mM of glucose in trisbuffer (pH = 7.5). The mixture was vortexed for 4 h, and then let them stand for 1 h. The prepared vesicles solution was passed through the column of sephadex G-50 by using trisbuffer (pH = 7.5) as the eluent to eliminate the free glucose. The concentration of **TPAI-C8** in the stock solution was 40 mM. The glucose-entrapping vesicles were collected. 10 μL vesicle stock solution, 2000 μL tris buffer (pH = 7.5), 500 μL enzyme solution (10 units per mL of hexokinase/glucose-6-phosphoate dehydrogenas and 2.0 mM ATP dissolved in the above Tris buffer) and 500 μL NADP solution (1.0 mM dissolved in the above Tris buffer) were added into the cuvette. The absorbance of NADPH at 340 nm was measured. Subsequently, 100 μL of Triton X-100 (5% v/v) was added into the cuvette and the absorbance at 340 nm was measured. The absorbance of

View Article Online
DOI: 10.1039/C8NJ01503A

NADPH at 340 nm was monitored. Subsequently, the vesicles were lysed by the addition of 100 μL of Triton X-100 (5% v/v) and the absorbance at 340 nm (A_{max}) was used to calculate the percent leakage [= $(A_t - A_0)/(A_{max} - A_0) \times 100$]. A_0 and A_t are the initial and intermediate absorbance, respectively.

The measurement of the critical vesicle concentration (CVC): The measurement of the critical vesicle concentration (CVC) was measured according to the reported literature.[49]

The measurement of CVC for TPAI-Cn: The CVC of **TPAI-Cn** was measured by the fluorescence emission of TPA buried in the vesicles. Briefly, the stock solution of **TPAI-Cn** was diluted to various desired concentrations (from 1 mM to 100 mM). The fluorescence spectra of all solutions were measured with the excitation wavelength at 380 nm, and the intensity values of all solutions at 450 nm were recorded to determine the CVC.

The measurement of CVC for TPEI-C8: The CVC of **TPEI-C8** was measured by the fluorescence emission of TPE buried in the vesicles. Briefly, the stock solution of **TPEI-C8** was diluted to various desired concentrations (from 10 μM to 1000 μM). The fluorescence spectra of all solutions were measured with the excitation wavelength at 380 nm, and the intensity values of all solutions at 480 nm were recorded to determine the CVC.

Cell culture: Hela cells were incubated in Dublecco's Minimum Eagle's Medium (DMEM, Hyclone) supplemented with 10% (v/v) fetal bovine serum (FBS, Gibco), 1 units/mL of penicillin (Sigma-Aldrich), and 0.1 mg/mL of streptomycin (Sigma-Aldrich) at 37 °C in a humidified atmosphere containing 5% CO_2.

Confocal imaging experiments: For co-staining experiments, Hela cells was incubated with **TPEI-C8** (50 μM) in Dublecco's Minimum Eagle's Medium (DMEM, Hyclone) for 4 h at 37 °C. After incubation, Hela cells were washed twice with PBS. Then, (500 μL) **Reddot1** was added to incubate for 5 min at 37 °C. Finally, Hela cells were washed twice with PBS before imaging.

Cytotoxicity assays: The cytotoxicity study of **TPEI-C8** was examined by MTT. Hela cells were seeded in the 96-well plate and treated for 24 h with different concentrations of **TPEI-C8** solutions (5, 10, 20, 40 and 80 μM). After the treatment, 20 μL PBS containing 5 mg/mL MTT was added to each well and the plate was incubated at 37 °C for 4 h. The purple formazan crystals were dissolved in 200 μL of DMSO, and the absorbance of each sample was measured on the multi-detection microplate reader (Bio-Rad 550) at 490 nm. The cell viability was calculated by the following formula: viability (%) = (mean absorbance value in treated wells/ mean absorbance value in control wells) × 100.

General procedure for the synthesis of the silver alkyl carboxylate: Sodium carboxylate was dissolved in de-ionized water. To the sodium carboxylate solution (0.2 M, 100 mL), a solution of $AgNO_3$ (0.405 M, 50 mL) was added dropwise under vigorous stirring. The precipitate compound was filtered, washed with de-ionized water and dried under vacuum. The desired product silver carboxylate was obtained as a white powder.

Synthesis of silver hexanoate: Following the general procedure, sodium hexanoate (2.76 g, 20.0 mmol) and $AgNO_3$ (3.44 g, 20.2 mmol) were used to obtain the desired product (4.07 g, 91.4%).

Synthesis of silver octanoate: Following the general procedure, sodium octanoate (3.32 g, 20.0 mmol) and $AgNO_3$ (3.44 g, 20.2 mmol) were used to obtain the desired product (4.69 g, 93.44%).

General procedure for the synthesis of the TPAI-C6, TPAI-C8, TPEI-C8: The silver carboxylate (0.1528 g, 0.9 mmol) was added to the aqueous solution of **TPAI-Br** or **TPEI-Br** (0.31 mmol) and the white precipitate immediately changed into a yellow brown precipitate. After being stirred at room temperature under dark for 24 h, the reaction mixture was filtered. The filtrate was stirred with 50.0 mg active carbon for 2 h to remove the trace silver precipitate and then concentrated under vacuum. The crude product was dissolved into dichloromethane, and was filtered to remove the excessive **TPAI-Br** or **TPEI-Br**. The filtrate was concentrated under vacuum, then the crude product was recrystallized with dichloromethane and diethyl ether to get light yellow solid and dried under vacuum to get the desired product.

Synthesis of the TPAI-C6: Following the general procedure, **TPAI-Br** (0.2358 g, 0.31 mmol), silver hexanoate (0.1528 g, 0.9 mmol) and de-ionized water (50.0 mL) were used to obtain the desired product (0.1983 g, 75%). ^{1}H NMR (D_2O-d_2, 400 MHz): δ = 0.77 (t, J = 7.2 Hz, 9H), 1.17 (s, 12H), 1.45 (m, 6H), 1.47 (t, J = 7.2 Hz, 9H), 2.03 (t, J = 7.6 Hz, 6H), 4.23 (m, 6H),7.31 (d, J = 9.2 Hz, 6H), 7.31(d, J = 9.2 Hz, 6H), 7.49(d, J = 8.8 Hz, 6H), 7.60 (d, J = 2.4 Hz, 3H), 7.75 (d, J = 2.0 Hz, 3H). ^{13}C NMR ($CDCl_3$-d, 100 MHz): δ = 15.5, 22.4, 26.4, 32.0, 38.5, 45.5, 120.6, 122.1, 123.2, 125.4, 130.6, 147.1 ppm. HRMS (ESI^+): calcd for $C_{33}H_{36}N_7^{3+}$ $[M-X]^+$ 530.3016, found 530.3027.

Synthesis of the TPAI-C8: Following the general procedure, **TPAI-Br** (0.2358 g, 0.31 mmol), silver octanoate (0.2259 g, 0.9 mmol) and de-ionized water (50.0 mL) were used to obtain the desired product (0.2413 g, 83%). ^{1}H NMR (D_2O-d_2, 400 MHz): δ = 0.70 (t, J =6.8 Hz, 9H), 1.14 (s, 24H), 1.38 (m, 6H), 1.46 (t, J = 7.2 Hz, 9H), 2.00 (t, J = 7.4 Hz, 6H), 4.22 (m, 6H), 7.31 (d, J = 8.8 Hz, 6H), 7.50 (d, J = 8.8 Hz, 6H), 7.61 (d, J = 2.0 Hz, 3H), 7.76 (d, J = 2.0 Hz, 3H). ^{13}C NMR ($CDCl_3$-d, 100 MHz): δ = 13.3, 14.8, 16.9, 22.2, 26.1, 29.1, 37.4, 45.5, 57.5, 121.4, 122.6, 123.5, 125.5, 130.4, 147.8, 183.3 ppm. HRMS (ESI^+): calcd for $C_{33}H_{36}N_7^{3+}$ $[M-X]^+$ 530.3016, found 530.3049.

Synthesis of the TPEI-C8: Following the general procedure, **TPEI-Br** (0.1781 g, 0.17 mmol), silver octanoate (0.1096 g, 0.66 mmol) and de-ionized water (50.0 mL) were used to obtain the desired product (0.2145, 79%).^{1}H NMR (D_2O-d_2, 400 MHz): δ = 0.74 (t, J = 7.0 Hz, 12H), 1.18(s, 16H), 1.4 (m, 8H), 1.47 (t, J = 7.2 Hz, 12H), 2.03 (t, J = 7.6 Hz, 8H), 4.23 (m, 8H), 7.31 (d, J = 8.8 Hz, 8H), 7.49 (d, J = 8.8 Hz, 8H), 7.60 (d, J = 2.4 Hz, 4H), 7.75 (d, J = 2.0 Hz, 4H). ^{13}C NMR (*CDOD*-d_4, 100 MHz): δ = 13.0, 14.1, 22.4, 26.2, 28.9, 29.3, 31.6, 45.2, 121.2, 121.8, 123.2, 132.6, 134.1, 143.5, 181.8 ppm. HRMS (ESI^+): calcd for $C_{33}H_{36}N_7^{3+}$ $[M-X]^+$ 712.3890, found 712.3885.

View Article Online
DOI: 10.1039/C8NJ01503A

Acknowledgements

This work was financially supported by grants from the National NSF of China (No. 21502129), China Postdoctoral Science Foundation Funded Project (2017M612956), and the National 111 Project of Introducing Talents of Discipline to Universities (No. B16033).

Notes and references

1. C. G. Palivan, R. Goers, A. Najer, X. Zhang, A. Car and W. Meier, *Chem. Soc. Rev.*, 2016, **45**, 377-411.
2. D. L. Perrier, L. Rems and P. E. Boukany, *Adv. Colloid. Interfac.*, 2017, **249**, 248-271.
3. J. Song, P. Huang, H. Duan and X. Chen, *Accounts. Chem. Res.*, 2015, **48**, 2506-2515.
4. P. Vader, E. A. Mol, G. Pasterkamp and R. M. Schiffelers, *Adv. Drug. Deliv. Rev.*, 2016, **106**, 148-156.
5. P. Xing and Y. Zhao, *Adv. Mater.*, 2016, **28**, 7304-7339.
6. E. W. Kaler, A. K. Murthy, B. E. Rodriguez and J. A. N. Zasadzinski, *Science*, 1989, **245**, 1371-1374.
7. Y. Chang, K. Yang, P. Wei, S. Huang, Y. Pei, W. Zhao and Z. Pei, *Angew. Chem. Int. Ed.,* 2014, **53**, 13126-13130.
8. Y. Chen, F. Qiao, Y. Fan, Y. Han and Y. Wang, *Langmuir,* 2017, **33**, 2760-2769.
9. M. Gao, X. Zhu, L. Wu and L. Qiu, *Biomacromolecules*, 2016, **17**, 2199-2209.
10. C. R. López-Barrón, D. Li, L. DeRita, M. G. Basavaraj and N. J. Wagner, *J. Am.Chem. Soc.*, 2012, **134**, 20728-20732.
11. M. Dubois, Th. Gulik-Krzywicki, J.-C. Dedieu, C. Vautrin, S. Désert, E. Perez and T. Zemb, *Nature*, 2001, **411**, 672-675.
12. Th. Zemb, M. Dubois, B. Demé and Th. Gulik-Krzywicki, *Science*, 1999, **283**, 816-819.
13. S. A. Wheaten, F. D. O. Ablan, B. L. Spaller, J. M. Trieu and P. F. Almeida, *J. Am. Chem. Soc.*, 2013, **135**, 16517-16525.
14. Y. Yang, L. Liu, X. Huang, X. Tan, T. Luo and W. Li, *Soft Matter*, 2015, **11**, 8848-8855.
15. C. Li, S. Zhang, J. Pang, Y. Wu and Z. Gu, *Adv. Funct. Mater*, 2015, **25**, 3764-3774.
16. W. W.-W. Hsiao, Y. Y. Hui, P.-C. Tsai and H.-C. Chang, *Acc. Chem. Res.*, 2016, **49**, 400-407.
17. Y. Tang, D. Lee, J. Wang, G. Li, J. Yu, W. Lin and J. Yoon, *Chem. Soc. Rev.*, 2015, **44**, 5003-5015.
18. W. Xu, Z. Zeng, J.-H. Jiang, Y.-T. Chang and L. Yuan, *Angew. Chem. Int. Ed.*, 2016, **55**, 13658-13699.
19. H. Zhu, J. Fan, J. Du and X. Peng, *Acc. Chem. Res.*, 2016, **49**, 2115-2126.
20. H.-S. Peng and D. T. Chiu, *Chem. Soc. Rev.*, 2015, **44**, 4699-4722.
21. Y. Xia, R. Zhang, Z. Wang, J. Tian and X. Chen, *Chem. Soc. Rev.*, 2017, **46**, 2824-2843.
22. M. Huang, R. Yu, K. Xu, S. Ye, S. Kuang, X. Zhu and Y. Wan, *Chem. Sci.*, 2016, **7**, 4485-4491.
23. J. Mei, Y. Hong, J. W. Y. Lam, A. Qin, Y. Tang and B. Z. Tang, *Adv. Mater.*, 2014, **26**, 5429-5479.
24. J. Luo, Z. Xie, J. W. Y. Lam, L. Cheng, H. Chen, C. Qiu, H. S. Kwok, X. Zhan, Y. Liu D. Zhu and B. Z. Tang, *Chem. Commun.*, 2001, 1740-1741.
25. J. Huang, Y. Yu, L. Wang, X. Wang, Z. Gu and S. Zhang, *ACS Appl. Mater. Interfaces*, 2017, **9**, 29030-29037.
26. C. W. T. Leung, Y. Hong, S. Chen, E. Zhao, J. W. Y. Lam and B. Z. Tang, *J. Am. Chem. Soc.*, 2013, **135**, 62-65.
27. J. Li, K. Liu, Y. Han, B. Z. Tang, J. Huang and Y. Yan, *ACS Appl. Mater. Interfaces*, 2016, **8**, 27987-27995.
28. K. K. Ng and G. Zheng, *Chem. Rev.*, 2015, **115**, 11012-11042.
29. G. Fan and D. Yan, *Sci. Rep.*, 2014, **4**, 4933.
30. G. Fan and D. Yan, *Adv. Opt. Mater.*, 2016, **4**, 2139-2147.
31. D. Yan and D. G. Evans, *Mater. Horiz.*, 2014, **1**, 46-57.
32. D. Yan, H. Yang, Q. Meng, H. Lin and M. Wei, *Adv. Funct. Mater.*, 2014, **24**, 587-594.
33. S. Li, Y. Lin and D. Yan, *J. Mater. Chem. C*, 2016, **4**, 2527-2534.
34. J. J. Garcia-Celma, L. Hatahet, W. Kunz, and K. Fendler, *Langmuir*, 2007, **23**, 10074-10080.
35. S. Dengler, G. J. T. Tiddy, L. Zahnweh and W. Kunz, *Colloid. Surface. A*, 2014, **457**, 414-418.
36. A. Renoncourt, N. Vlachy, P. Bauduin, M. Drechsler, D. Touraud, J.-M. Verbavatz, M. Dubois, W. Kunz, and B. W. Ninham, *Langmuir*, 2007, **23**, 2376-2381.
37. R. Klein, M. Kellermeier, D. Touraud, E. Müller and W. Kunz, *J. Colloid Interf. Sci.*, 2013, **392**, 274-280.
38. R. Klein, D. Touraud and W. Kunz, *Green Chem.*, 2008, **10**, 433–435.
39. N. Vlachy, C. Merle, D. Touraud, J. Schmidt, Y. Talmon, J. Heilmann and W. Kunz, *Langmuir*, 2008, **24**, 9983-9988.
40. D. Rengstl, B. Kraus, M. V. Vorst, G. D. Elliott and W. Kunz, *Colloid. Surface. B*, 2014, **123**, 575-581.
41. N. Vlachy, M. Drechsler, J.-M. Verbavatz, D. Touraud and W. Kunz, *J. Colloid Interf. Sci.*, 2008, **319**, 542-548.
42. G. Li, S. Zhang, N. Wu, Y. Cheng and J. You, *Adv. Funct. Mater.*, 2014, **24**, 6204-6209.
43. A. Shioi and T. A. Hatton, *Langmuir*, 2002, **18**, 7341-7348.
44. S. C. Kinsky, J. A. Haxby, D. A. Zopf, C. R. Alving and C. B. Kinsky, *Biochemistry*, 1969, **8**, 4149-4158.
45. Y. Cheng, G. Li, Y. Liu, Y. Shi, G. Gao, D. Wu, J. Lan and J. You, *J. Am. Chem. Soc.*, 2016, **138**, 4730-4738.
46. T. Peng, N.-K. Wong, X. Chen, Y.-K. Chan, D. H.-H. Ho, Z. Sun, J. J. Hu, J. Shen, H. EI-Nezami and D. Yang, *J. Am. Chem. Soc.*, 2014, **136**, 11728-11734.
47. N. Sinha, T. T. Y. Tan, E. Peris and F. E. Hahn, *Angew. Chem. Int. Ed.*, 2017, **56**, 7393-7397.
48. N. Sinha, L. Stegemann, T. T. Y. Tan, N. L. Doltsinis, C. A. Strassert and F. E. Hahn, *Angew. Chem. Int. Ed.*, 2017, **56**, 2785-2789.
49. J. Huang, Y. Yu, L. Wang, X. Wang, Z. Gu and S. Zhang, *ACS Appl. Mater. Interfaces*, 2017, **9**, 29030-29037.

View Article Online
DOI: 10.1039/C8NJ01503A

Graphic Abstract

Cation–anion interaction directed formation of functional vesicles and their biological application for nucleus-specific imaging

Qunshou Kong, Weihua Zhuang, Gaocan Li, Qing Jiang* and Yunbing Wang*

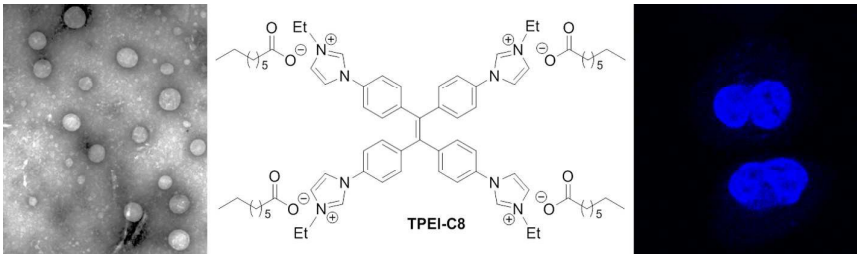

A strategy for construction of counterion-induced vesicles in aqueous media has been described by imidazolium salts with multiple imidazolium moieties and alkyl carboxylate counteranions. Furthermore, the imidazolium salt with an aggregation induced emission (AIE) fluorophore exhibits highly specific nucleus imaging in living cells.